Photon-Assisted Oxygen Diffusion and Oxygen-Related Traps in Organic Semiconductors

*Hikmet Najafov, Daniel Mastrogiovanni, Eric Garfunkel, Leonard C. Feldman, and Vitaly Podzorov**

Organic molecular crystals represent an excellent platform for fundamental studies of optoelectronic properties of organic semiconductors.[1] Rubrene, in particular, has attracted significant attention due to a very low density of charge traps, record-high charge carrier mobility, and a very large micrometer-scale exciton diffusion length.[2,3] In this study, using rubrene as a model compound questions related to the interaction of crystalline organic semiconductors with oxygen are addressed. Although the chemistry of photo-oxidation of rubrene in solution and gas phases is understood based on self-sensitized photo-oxidation (see for example, Ref.[4]), the mechanism of oxygen incorporation and its effect on the photophysical properties of crystalline rubrene still remain controversial. Mitrofanov et al.[5] identified an oxygen-related in-gap band in photo-oxidized rubrene by means of a two-photon photoluminescence excitation spectroscopy and showed that oxygen is concentrated near the surface of the crystals. Krellner et al.[6] revealed that an oxygen-related impurity forms an acceptor-like in-gap state in rubrene with an energy ≈0.28 eV above the highest occupied molecular orbital (HOMO). X. Song et al.[7] used photoemission and X-ray absorption spectroscopies to show that the HOMO of oxidized rubrene is ≈1 eV deeper than that of pure rubrene and hence can not account for formation of acceptor-like states within the bandgap. Therefore, in this contribution, we set out to answer the following questions: What triggers oxygen incorporation in molecular crystals? What is its effect on the conductivity of these materials? What dictates the depth distribution of oxygen defects?

In this paper, a highly sensitive trap characterization technique based on wavelength- and polarization-resolved photocurrent excitation spectroscopy of single crystalline organic semiconductors is developed and applied for the first time. The method reveals that even a brief illumination of organic molecular crystals in an oxygen atmosphere triggers a long-term oxygen diffusion that continues in the dark and results in formation of oxygen-related traps in the crystal at the length scale $\approx\alpha^{-1}$, where α is the light absorption coefficient. For example, in rubrene, no oxygen diffusion occurs in the dark without an initial photoexcitation, even if the samples are stored in pure oxygen. Our studies show that oxygen incorporation reduces both the dark- and photoconductivity of rubrene and leads to qualitative changes in the photocurrent excitation spectra that can be used for the characterization of traps in molecular crystals.

We take advantage of the anisotropic molecular packing of rubrene which results in an optical absorption coefficient, $\alpha(\lambda,\theta)$, that is both wavelength, λ, and polarization angle, θ, dependent, as is the case in many molecular crystals.[8] Here, θ is defined as an angle between the polarization of linearly polarized light and the *a*-axis of rubrene (light is always at normal incidence to the (*a*,*b*) face) (**Figure 1**). Specifically, α reaches maxima for polarization along the high-mobility *b*-axis ($\theta = 90°$) and minima for polarization along the *a*-axis of rubrene ($\theta = 0$). That is, $\alpha(\theta)$ looks like a harmonic function with a periodicity π superimposed on a positive constant. In addition, vibronic modes of rubrene cause large modulations of α with wavelength (Figure 1b). This allows us to continuously vary the characteristic light penetration length in the *c*-axis direction according to the Beer–Lambert law in a wide range by changing λ or θ: $\alpha^{-1}(\theta,\lambda) = 1$–$140$ μm. These properties are used to study the distribution of oxygen-induced traps in rubrene by measuring the photoconductivity, $\sigma(\theta,\lambda)$, which is then compared with $\alpha(\theta,\lambda)$.

Organic crystals used in this study fall in the three major categories: (a) the so-called pristine high-purity rubrene with negligible trap density and a large built-in surface conduction channel ($\sigma_{\text{built-in}} \approx 10^{-9}$–$10^{-8}$ S per square in ungated free-standing crystals);[9] (b) medium-purity crystals, in which the built-in surface conduction channel is suppressed by traps (the so-called, trap-dominated crystals); and (c) intentionally photo-oxidized crystals, in which the trap density can be increased in a controlled fashion. To avoid impurities previously described in Ref. [10] and eliminate oxidation of the harvested crystals, we have performed the crystal growth in the dark and minimized exposure of crystals to light during handling. Electrical contacts have been prepared by depositing colloidal graphite paint on the largest natural facet of the crystals (the (*a*,*b*) facet) in a coplanar configuration, defining channel length, L = 1–5 mm, and width, W = 1–3 mm (Figure 1a). Conductivity was probed along the high-mobility *b*-axis using Keithley instruments. The

Dr. H. Najafov, Prof. V. Podzorov
Physics Department, Rutgers University
Piscataway, NJ 08854, USA
E-mail: podzorov@physics.rutgers.edu
D. Mastrogiovanni, Prof. E. Garfunkel
Department of Chemistry
Rutgers University
Piscataway, NJ 08854, USA
Dr. H. Najafov, Prof. E. Garfunkel, Prof. L. C. Feldman, Prof. V. Podzorov
Institute for Advanced Materials and Devices for Nanotechnology
Rutgers University
Piscataway, NJ 08854, USA

DOI: 10.1002/adma.201004239

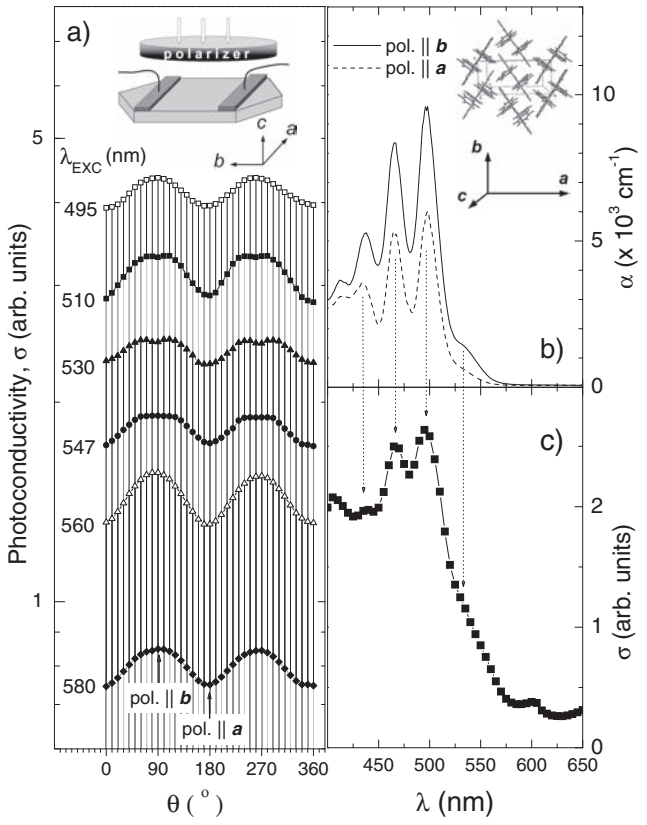

Figure 1. a) Polarization dependence of the photoconductivity in pristine (high-purity) rubrene crystal at various excitation wavelengths showing the "normal" character of modulations. Sample geometry is shown in the inset. The light is normally incident at the (*a*,*b*) facet of the crystal (structure shown in (b)). Photocurrent maxima are observed at $\theta = 90°$, 270°, etc., corresponding to *b*-polarized light, and minima at $\theta = 0$, 180°, etc., corresponding to *a*-polarized light. The corresponding ranges of light penetration length for polarization changing from *b* to *a* are: $\alpha^{-1}(\lambda)$ = 1.04–1.66 μm (495 nm), 2.0–3.4 μm (510 nm), 6.7–13.6 μm (530 nm), 12.2–32.4 μm (547 nm), 33.2–78.2 μm (560 nm), 97.5–141.5 μm (580 nm). b) Experimental absorption spectra of rubrene, $\alpha(\lambda)$, for *b*- and *a*-polarized light and molecular packing in the (*a*,*b*) plane of rubrene (inset). c) Photocurrent excitation spectrum of pristine rubrene crystals.

thickness of all the crystals used in this study was macroscopic: 0.5–2 mm. A typical voltage between the contacts in the photocurrent measurements was 20 V. Photo-oxidation and all the measurements were performed in a hermetic chamber equipped with optical windows and gas/instrumentation feedthroughs. Photo-oxidation was carried out by illuminating the samples in an ultrahigh purity O_2 atmosphere for 2 h with a white light at an integrated flux similar to solar radiation: Φ_0 = 85 mW cm^{-2} (Xe lamp with a blocked UV component). For the photoconductivity measurements, light with a much smaller flux was used: the (*a*,*b*) facet of the crystals kept in Ar was illuminated at a normal incidence with monochromatic light obtained by transmitting illumination from a halogen lamp with a smooth white spectrum through a monochromator or narrow (10-nm) band-pass filters; the photoexcitation flux was typically 20 μW cm^{-2}. Polarization of the incident light was varied with a linear polarizer placed in front of the sample.

Figure 1a shows the polarization dependence of the photoconductivity, $\sigma(\theta)$, measured under monochromatic photoexcitation in the range 495–580 nm (a constant dark current due to the built-in channel was subtracted, so that pure photoconductivity is shown in Figure 1 and hereafter). This dataset shows that in macroscopically thick rubrene crystals, photoconductivity, $\sigma(\theta)$, exhibits small periodic modulations with polarization angle that have an amplitude: $\eta_\sigma = (I_{MAX} - I_{MIN})/I_{MAX} \approx$ 9–16%, where I_{MAX} and I_{MIN} are the photocurrent at the maxima and minima in Figure 1a, corresponding to the photocurrents for *b*- and *a*-polarized photoexcitation, respectively. In high-purity (pristine) rubrene, these conductivity modulations are always much smaller than the corresponding modulations of the absorption coefficient, $\eta_\alpha = (\alpha_b - \alpha_a)/\alpha_b$ = 32–63% (this range is indicated for λ = 495–580 nm), and the maxima and minima in $\sigma(\theta)$ always occur at polarizations along the *b* and *a* axes, respectively, i.e., the angular positions of maxima and minima in $\sigma(\theta)$ match those in $\alpha(\theta)$. We refer to such behavior as "normal modulations" of photoconductivity. The photocurrent excitation spectrum (PCE) of pristine rubrene also shows a striking correlation with the absorption spectrum in terms of the positions of all vibronic sidebands (Figure 1c), although the relative modulations in $\sigma(\lambda)$ are again much smaller than those in $\alpha(\lambda)$ (compare Figure 1b and c). Overall, in pristine crystals we observe a direct correlation of $\sigma(\lambda,\theta)$ with $\alpha(\lambda,\theta)$ in terms of the positions of the maxima and minima, while the modulation amplitude (the "contrast") of σ is considerably reduced compared to that of α.

At first glance, such behavior is unexpected in macroscopically thick crystals, because 100% of the incident photons are absorbed in the material at any θ and λ, which should result in a θ- and λ-independent photocurrent, assuming that the photoconductivity is a bulk phenomenon. As shown in detail elsewhere,[3] bulk photoconductivity in pristine rubrene is negligible, and up to 90% of the total photocurrent originates from a long-range diffusion of excitons (3–8 μm) and their surface dissociation, which provides a dominant contribution to the photoconductivity. For a *b*-polarized photoexcitation (i.e., at the smallest light penetration length), more excitons are generated within the exciton diffusion length below the surface of the crystal than for an *a*-polarized photoexcitation, leading to the observed correlation of the extrema in $\sigma(\lambda,\theta)$ and $\alpha(\lambda,\theta)$ in pristine rubrene.[3]

Figure 2a,d show photoconductivity $\sigma(\lambda,\theta)$ measured in a trap-dominated sample. A strikingly different behavior is observed. Modulations of the photocurrent with θ and λ are inverted, i.e., they anticorrelate with the absorption function $\alpha(\lambda,\theta)$. We refer to such behavior as "antimodulations". Closer inspection of Figure 2a reveals that each $\sigma(\theta)$ curve is a superposition of a normal and antimodulated characters added up with different weights that depend on λ. For example, $\sigma(\theta)$ at λ = 560 and 580 nm resemble the normal modulations in pristine crystals, with "eaten up" maxima at $\theta = 90°$ and 270° (one can clearly see dips in the 560 nm curve at the positions where the maxima would be expected in pristine rubrene; the dips become more pronounced in 580 nm curve). At 547 nm excitation, very large antimodulated dips develop at 90° and 270°, while the remnants of the normal modulations can be

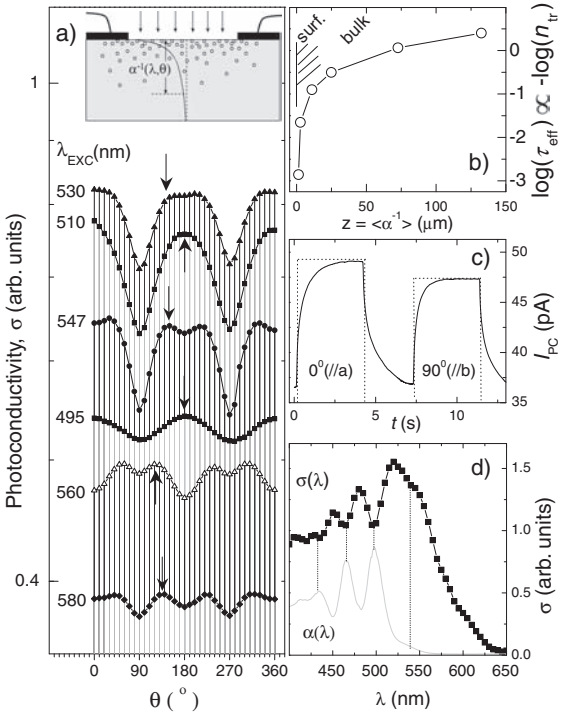

Figure 2. a) Polarization dependence of the photoconductivity in a trap-dominated rubrene crystal at various excitation wavelengths showing the "antimodulated" behavior. Inset is a sketch of a device cross section with traps distributed near the surface and a light penetration profile that has a characteristic depth $\alpha^{-1}(\lambda,\theta)$. b) Distribution of trap-limited carrier lifetimes and densities (in arbitrary units) in a trap-dominated sample as a function of the depth into the crystal ($z = 0$ corresponds to the surface of the crystal). See details in the Supporting Information. c) Time dynamics of the photocurrent induced by 580 nm rectangular pulsed photoexcitations polarized along *a*- and *b*-axes of the crystal. d) A photocurrent excitation spectrum of a trap-dominated rubrene crystal (solid squares) with the absorption spectrum (grey solid line) shown for comparison.

recognized as "wings" at 0–30° and 330–360° and a "saddle" at 150–210°. For even shorter wavelengths (495, 510, and 530 nm) corresponding to the smallest light penetration lengths, an antimodulated behavior completely dominates $\sigma(\theta)$. In general, the observed tendency is such that the smaller the light penetration length, α^{-1}, the stronger the observed antimodulation behavior in $\sigma(\theta)$ of trap-dominated samples. Importantly, the absolute value of photoconductivity in trap-dominated samples showing antimodulations is always much smaller than σ of pristine crystals, which suggests a trap-related origin of the observed antimodulations.

We believe that this interesting effect is due to interaction of photogenerated carriers with charge traps. Indeed, in trap-dominated samples, long-range exciton diffusion and the surface photocurrent are greatly suppressed by traps, leading to the total photocurrent dominated by the bulk dissociation of short-lived excitons. Hence, photoconductivity in this case has a bulk character with photocarriers distributed in the crystal following the Beer–Lambert exponential decay of light intensity. These carriers interact with traps that typically have a higher density near the surface of the crystal (inset at Figure 2a).

A better understanding of this phenomenon can be gained from the time dynamics of the photoconductivity under a pulsed photoexcitation. Figure 2c shows a typical time-resolved σ response of trap-dominated rubrene under a rectangular 580 nm pulsed photoexcitation polarized along *a* ($\theta = 0°$) and *b* ($\theta = 90°$) axes. It can be seen that light with a smaller penetration length (*b*-polarized) yields σ with a relatively smaller amplitude and shorter build-up and decay times, indicating a shortening of the effective carrier lifetime. According to Shockley and Reed, trap-limited carrier lifetime, τ_{eff}, is inversely proportional to the trap density, n_{tr}: $\tau_{eff} \propto n_{tr}^{-1}$.[11] Hence, antimodulations in photoconductivity $\sigma(\theta,\lambda)$ must arise from carrier trapping, which becomes more efficient when the depth of photoexcitation $\alpha^{-1}(\theta,\lambda)$ better matches the characteristic depth of the trap distribution in the crystal (sketch in Figure 2a). Using the polarization dependencies $\sigma(\theta)$ in Figure 2a and the Shockley–Reed equation (see Supporting Information for details), it is possible to reconstruct the spatial distribution of traps in the crystal and show that traps may extend for up to ≈100 μm into the crystal with a density increasing rapidly toward the sample's surface at $z = 0$ (Figure 2b).

We next demonstrate that a gradual evolution of $\sigma(\theta)$ dependence from normal to antimodulated can be observed in situ in individual samples subjected to photo-oxidation in a controlled environment. Pristine samples were measured and then photo-oxidized (white light, integral power 85 mW cm^{-2}, 2 h in ultra-high purity O_2). After this initial step of photo-oxidation, the samples were allowed to relax in the dark for 30 min and then the photoconductivity, $\sigma(\theta)$, was measured every 2 h using a 495 nm excitation with a much smaller power (20 μW cm^{-2}). During the 2 h waiting periods, the samples were kept in an O_2 atmosphere in the dark.

Figure 3a shows the resulting $\sigma(\theta)$ recorded at different times after the photo-oxidation. The starting state of the sample is pristine (normal modulations). Temporal variation of the θ-averaged photoconductivity level is shown in Figure 3b. The initial large drop of σ corresponds to the traps introduced during the photo-oxidation step, also manifested by the appearance of a plateau at $\theta = 60$–$120°$ on the 2 h curve in Figure 3a. Note that the plateau gradually evolves into a dip and then into a complete antimodulated $\sigma(\theta)$ as the sample spends time in O_2 in the dark (after the photo-oxidation step). It is important to note that without photo-oxidation at the beginning, storing pristine rubrene crystals in O_2 atmosphere or air in the dark does not lead to any modifications of the absolute value or polarization dependence of the photoconductivity. This remarkable observation suggests that the initial step of a brief illumination in O_2 triggers the process of a gradual diffusion of molecular oxygen into the organic lattice that occurs in the dark on the time scale of many hours or days. Special control experiments show that both bandgap illumination and the presence of O_2 are necessary for the observed effect to occur (Supporting Information).

The appearance of a plateau on the 2 h curve suggests that oxygen species penetrate into the crystal to the depth of approximately $\alpha^{-1}{}_{495\ nm}(\theta = 60°, 120°) \approx 1.2$ μm already during the initial step of photo-oxidation. Gradual progression of the plateau into the dip indicates that oxygen keeps incorporating into the crystal long after the initial photo-oxidation step. As seen in Figure 3a,b, oxygen incorporation reduces the level of

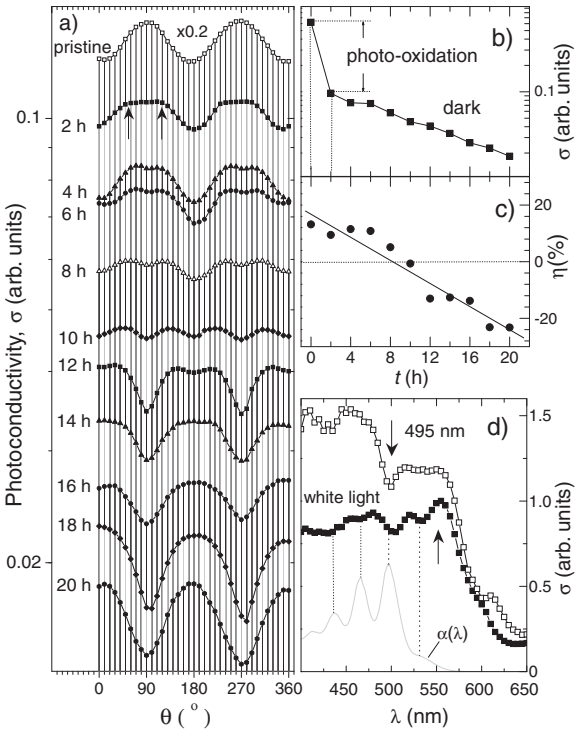

Figure 3. a) Polarization dependencies of the photoconductivity in photo-oxidized rubrene crystal measured at 495 nm every 2 h after the photo-oxidation. During each 2 h waiting period the sample has been stored in the dark in O_2 atmosphere. The top-most curve corresponds to the pristine crystal before the photo-oxidation. b) Variation of the average level of the photoconductivity with time during and after the photo-oxidation corresponding to the curves in (a). c) Variation of the modulation amplitude η_σ with time: change of sign at 8–10 h manifests a crossover from normal to antimodulated behavior. d) Photocurrent excitation spectra $\sigma(\lambda)$ of rubrene after photo-oxidation with white (solid squares) and 495 nm monochromatic (open squares) light, showing a "spectral burning" effect. Absorption spectrum (grey solid line) is shown for comparison.

photoconductivity of rubrene by more than an order of magnitude. At the same time it changes the character of the $\sigma(\theta)$ dependence qualitatively: a crossover from normally modulated (pristine) to a completely antimodulated (trap-dominated) $\sigma(\theta)$ occurs. Variations of the modulation amplitude, η_σ, can be used to quantify the time scale of this process (Figure 3c). It takes about 10 h for a complete antimodulation behavior to develop, which corresponds to the curve with an apparent "period doubling", or $\eta_\sigma \approx 0$ (the 10 h curve at Figure 3a).

Similar to the case of trap-dominated samples, photo-oxidized rubrene shows an antimodulated $\sigma(\lambda)$ spectra (Figure 3d, solid squares). Note that the onset of anticorrelations with respect to $\alpha(\lambda)$ occurs at 560 nm (shown by the upward arrow), which corresponds to the red edge of rubrene absorption. This suggests that (a) oxygen diffusion can occur at the length scale of $\alpha^{-1}(560\text{ nm}) \approx 50\ \mu\text{m}$, and (b) oxygen does not penetrate deeper than the optical absorption edge of rubrene. The last point is very interesting because it suggests that oxygen penetration is programmed by the penetration length of light, $\alpha^{-1}(\lambda)$, used for the photo-oxidation. It implies that using monochromatic light for photo-oxidation should result in the effect of "spectral burning" in $\sigma(\lambda)$ spectra of organic semiconductors. Indeed, we have observed a clear dip in $\sigma(\lambda)$ of rubrene photo-oxidized using a monochromatic light (500 nm, 6 mW cm^{-2}, 8 h in ultra-high purity O_2) (Figure 3d, open squares). The appearance of only one sharp dip in the spectrum at about 500 nm indicates that incorporated traps are distributed within 1–2 μm below the surface of the crystal.

While the detailed mechanism of this effect requires further investigation, it is likely that the observed long-term O_2 diffusion relies on formation of "seeds", the defects (perhaps, endoperoxide or epoxy rubrene molecules[12]) created at a low density in the bulk during the initial step of photo-oxidation and distributed at length scale comparable to the light penetration length $\alpha^{-1}(\theta,\lambda)$. These seeds create pathways for a slow diffusion of molecular oxygen in the dark, perhaps facilitated by the local lattice distortion and strain associated with the presence of structurally distorted oxidized seed molecules.[13] The hindering factor for the oxygen diffusion in pristine crystals in the dark is a lack of defects on a clean, densely packed rubrene surface, unless it is photo-oxidized. Ongoing field-effect measurements of oxygenated rubrene reveal significant threshold voltage shifts corresponding to the density of oxygen-induced traps in the accumulation channel of up to 10^{12} cm^{-2}. This density, however, is still much smaller than the density of rubrene molecules in the channel (10^{14} cm^{-2}), indicating that structural modifications of oxygenated crystals are unlikely.

In conclusion, a novel methodology of trap diagnostics in semiconducting molecular crystals based on correlations between photoconductivity and light absorption coefficient is reported. Using this method it is discovered that illumination of organic crystals with a bandgap light in the presence of molecular oxygen triggers a long-term diffusion of O_2 in the dark. The depth scale of this oxygen diffusion is set by the light penetration length, $\alpha^{-1}(\theta,\lambda)$. The results show that photo-oxidation and subsequent oxygen diffusion lead to more than an order of magnitude decrease of dark- and photoconductivity of rubrene due to formation of oxygen-related traps.

Supporting Information

Supporting Information is available from the Wiley Online Library or from the author.

Acknowledgements

This work was financially supported by a NSF ARRA CAREER award under Grant No. DMR-0843985 and the Industrial Technology Research Grant Program 09E51007d (NEDO). We thank E. Chandross for helpful and stimulating discussions.

Received: November 17, 2010
Published online: January 21, 2011

[1] R. W. I. de Boer, M. E. Gershenson, A. F. Morpurgo, V. Podzorov, *Phys. Stat. Solidi* **2004**, *201*, 1302.
[2] V. Podzorov, E. Menard, A. Borissov, V. Kiryukhin, J. A. Rogers, M. E. Gershenson, *Phys. Rev. Lett.* **2004**, *93*, 086602.

[3] H. Najafov, B. Lee, Q. Zhou, L. C. Feldman, V. Podzorov, *Nat. Mater.* **2010**, *9*, 938.
[4] V. Nardello, M.-J. Marti, C. Pierlot, J.-M. Aubry, *J. Chem. Educ.* **1999**, *76*, 1285.
[5] O. Mitrofanov, D. V. Lang, C. Kloc, M. J. Wikberg, T. Siegrist, W.-Y. So, M. A. Sergent, A. P. Ramirez, *Phys. Rev. Lett.* **2006**, *97*, 166601.
[6] C. Krellner, S. Haas, C. Goldmann, K. P. Pernstich, D. J. Gundlach, B. Batlogg, *Phys. Rev. B* **2007**, *75*, 245115.
[7] X. Song, L. Wang, Q. Fan, Y. Wu, H. Wang, C. Liu, N. Liu, J. Zhu, D. Qi, X. Gao, A. T. S. Wee, *Appl. Phys. Lett.* **2010**, *97*, 032106.
[8] M. Pope, C. E. Swenberg, *Electronic Processes in Organic Crystals and Polymers*, 2nd ed., Oxford University Press, New York **1999**.
[9] V. Podzorov, V. M. Pudalov, M. E. Gershenson, *Appl. Phys. Lett.* **2004**, *85*, 6039.
[10] R. Zeis, C. Besnard, T. Siegrist, C. Schlockermann, X. L. Chi, C. Kloc, *Chem. Mater.* **2006**, *18*, 244.
[11] W. Shockley, W. T. Read, *Phys. Rev.* **1952**, *87*, 835.
[12] L. Tsetseris, S. T. Pantelides, *Org. Electron.* **2009**, *10*, 333.
[13] D. Käfer, L. Ruppel, G. Witte, Ch. Wöll, *Phys. Chem. Chem. Phys.* **2005**, *7*, 2850.